International Journal on Magnetic Particle Imaging
Vol 2, No 1, Article ID 1607002, 5 Pages

Infinite Science Publishing

Research Article

Optimized Compression of MPI System Matrices Using a Symmetry-Preserving Secondary Orthogonal Transform

Marco Maass[a,*] · Klaas Bente[b] · Mandy Ahlborg[b] · Hanne Medimagh[b] · Huy Phan[a] · Thorsten M. Buzug[b] · Alfred Mertins[a]

[a]Institute for Signal Processing, University of Lübeck, 23562 Lübeck, Germany
[b]Institute of Medical Engineering, Universtity of Lübeck, 23562 Lübeck, Germany
*Corresponding author, email: maass@isip.uni-luebeck.de

Received 27 November 2015; Accepted 13 June 2016; Published online 8 July 2016

Abstract

In this paper, we study the compression of the magnetic particle imaging system matrix for imaging setups in which a field free point is moved along a Lissajous trajectory. We show that a large number of zeros in the simulated transformed system matrix is obtained when orthogonal transforms applied to the spatial domain have only symmetric and antisymmetric basis functions. For measured system matrices, this property only holds approximately, because of noise induced by the scanner hardware. The required symmetry properties are naturally fulfilled by some standard orthogonal transforms such as the type-two discrete cosine transform and the discrete Chebychev transform. However, these transforms are not yet optimal for compressing system matrices, and we propose a new method to obtain better transforms that retain the required symmetry properties.

I. Introduction

The tracer-based imaging method magnetic particle imaging (MPI) allows one to measure the spatial distribution of super-paramagnetic iron oxid nanoparticles (SPIONs) [1]. A common approach to image the SPIONs' distribution in a two- or three-dimensional field of view (FOV) is the field free point (FFP) method [1]. The FFP is generated by the selection field and is the area where the SPIONs contribute most to the measured voltage signal. The dynamic drive field moves the FFP along a trajectory. A widely used trajectory is the Lissajous trajectory. In this paper we focus on the FFP method with two dimensional Lissajous trajectories. For the calculation of the spatial particle concentration from the voltage signal, a system matrix based reconstruction is widely used [2]. Since system matrices can be very large in size and thus consume a huge amount of memory in workspace, and because the image reconstruction can be significantly speeded up for sparse system matrices, it is of interest to compress them [3]. The idea is to compact the information on the system matrix into a few nonzero coefficients by using orthogonal transforms. The work in [3] considered the discrete Chebychev transform (DTT) and the discrete cosine transform of type-two (DCT-II) for this purpose and showed that a significant compression can be achieved for system matrices in MPI with a FFP that moves along a Lissajous trajectory. In this paper, we study the relationship between the symmetries of the applied transform and the compressibility of the system matrices. Based on the results, we introduce an effective compression method for system matrices.

10.18416/ijmpi.2016.1607002

II. Material and Methods

II.I. MPI system function

In MPI, the relationship between the measured voltage signal $u_\ell(t)$ of the ℓ-th receive channel and the particle concentration $c(\boldsymbol{r})$ is usually described by the Fourier series expansion of $u_\ell(t)$ with Fourier coefficients

$$\hat{u}_{\ell,k} = \int_\Omega \hat{s}_{\ell,k}(\boldsymbol{r}) c(\boldsymbol{r}) d\boldsymbol{r}, \tag{1}$$

where $\hat{s}_{\ell,k}(\boldsymbol{r})$ denotes the k-th system function component of receive channel ℓ, and Ω describes the FOV. The system function components are defined by

$$\hat{s}_{\ell,k}(\boldsymbol{r}) = -\hat{a}_{\ell,k} \frac{\mu_0}{T} \int_0^T \frac{\partial}{\partial t} \overline{\boldsymbol{m}}(\boldsymbol{r},t) \cdot \boldsymbol{p}_\ell(\boldsymbol{r}) e^{-2\pi \mathrm{i} \frac{kt}{T}} dt, \tag{2}$$

where $\hat{a}_{\ell,k}$ describes the transfer function of the receive chain, $\overline{\boldsymbol{m}}(\boldsymbol{r},t)$ is the mean magnetic moment, $\boldsymbol{p}_\ell(\boldsymbol{r})$ denotes the coil sensitivity, and T is the period. Under the assumption of isotropic SPIONs with instantaneous relaxation the mean magnetic moment is described by [4]

$$\overline{\boldsymbol{m}}(\boldsymbol{r},t) = \overline{m}(\|\boldsymbol{H}(\boldsymbol{r},t)\|) \frac{\boldsymbol{H}(\boldsymbol{r},t)}{\|\boldsymbol{H}(\boldsymbol{r},t)\|}. \tag{3}$$

Here, $\boldsymbol{H}(\boldsymbol{r},t)$ denotes the applied magnetic field and is given by $\boldsymbol{H}(\boldsymbol{r},t) = \boldsymbol{H}^S(\boldsymbol{r}) + \boldsymbol{H}^D(t)$, the superposition of the drive field $\boldsymbol{H}^D(t)$ and the selection field $\boldsymbol{H}^S(\boldsymbol{r})$, and $\overline{m}(z)$ denotes the magnitude of the mean magnetic moment [2]. If we further assume that all coils are aligned orthogonal to each other and that the sensitivity profiles of the coils are uniform, then the system Eq. (2) can be reduced to

$$\hat{s}_{\ell,k}(\boldsymbol{r}) = -\hat{a}_{\ell,k} \frac{\mu_0}{T} \int_0^T \frac{\partial}{\partial t} \overline{m}_\ell(\boldsymbol{r},t) e^{-2\pi \mathrm{i} \frac{kt}{T}} dt. \tag{4}$$

Here, we assume that $\ell = 0$ and $\ell = 1$ correspond to the y- and x-directions, respectively. The two-dimensional drive field for the Lissajous trajectory is defined by

$$\boldsymbol{H}^D(t) = \begin{pmatrix} H_x^D(t) \\ H_y^D(t) \end{pmatrix} = \begin{pmatrix} A_x \sin(2\pi f_x t) \\ A_y \sin(2\pi f_y t) \end{pmatrix}. \tag{5}$$

To obtain a periodic drive field, the frequency ratio $f_x/f_y = K_y/K_x$ has to be rational with $K_x, K_y \in \mathbb{N}$. The basis frequency is defined by $f_B := f_x K_x = f_y K_y$ and the period reads $T = \mathrm{lcm}(K_x, K_y)/f_B$, where lcm is the least common multiple of the frequency-ratio parameters. The spatial encoding is realized by the selection field

$$\boldsymbol{H}^S(\boldsymbol{r}) = \boldsymbol{G}\boldsymbol{r} \quad \text{with} \quad \boldsymbol{G} = \begin{pmatrix} G_x & 0 \\ 0 & G_y \end{pmatrix}. \tag{6}$$

II.II. Symmetries in the system function

In [4] it was shown that the following symmetries for an ideal two-dimensional drive field $\boldsymbol{H}_D(t)$ with even K_x, odd K_y, and period T hold for all $\tau \in \mathbb{R}$:

$$\begin{aligned} \begin{pmatrix} H_x^D(\tau) \\ H_y^D(\tau) \end{pmatrix} &= \begin{pmatrix} H_x^D\left(\frac{T}{2} - \tau\right) \\ -H_y^D\left(\frac{T}{2} - \tau\right) \end{pmatrix} \\ &= \begin{pmatrix} -H_x^D\left(\frac{T}{2} + \tau\right) \\ H_y^D\left(\frac{T}{2} + \tau\right) \end{pmatrix} = \begin{pmatrix} -H_x^D(T - \tau) \\ -H_y^D(T - \tau) \end{pmatrix}. \end{aligned} \tag{7}$$

With the assumption of an ideal drive field, the following theorem has been proven in [4].

Theorem 1 For an ideal coil configuration, isotropic SPIONs with instantaneous relaxation behavior, even K_x and odd K_y, the following symmetries hold for all components of two-dimensional signal functions

$$\begin{aligned} \tilde{m}_{\ell,k}(-r_x, r_y) &= (-1)^{k+\ell} \tilde{m}_{\ell,k}(r_x, r_y), & k \in \mathbb{N}_0, \\ \tilde{m}_{\ell,k}(r_x, -r_y) &= (-1)^{k+\ell} \left(\tilde{m}_{\ell,k}(r_x, r_y)\right)^*, & k \in \mathbb{N}_0, \end{aligned} \tag{8}$$

where * describes the complex conjugation and $\tilde{m}_{\ell,k}(\boldsymbol{r}) = \hat{s}_{\ell,k}(\boldsymbol{r})/\hat{a}_{l,k}$ is the signal function independent of the transfer function $\hat{a}_{l,k}$.

In real-world applications, the Fourier coefficients $\hat{u}_{\ell,k}$ of the sampled periodic signal $u_\ell(t_n)$ will be calculated using the discrete Fourier transform with the sampled time points

$$t_n = \frac{nT}{N_t} \tag{9}$$

with $n \in [0, 1, \ldots, N_t - 1]$ in one period T and $N_t \in \mathbb{N}$.

The spatial discretization will keep the symmetries in Eq. (8) if the grid points (r_x^u, r_y^v) are located at

$$\begin{aligned} r_x^u &= -\frac{A_x}{G_x} + 2\frac{N_x - 0.5 - u}{N_x} \frac{A_x}{G_x} \quad \text{and} \\ r_y^v &= -\frac{A_y}{G_y} + 2\frac{N_y - 0.5 - v}{N_y} \frac{A_y}{G_y} \end{aligned} \tag{10}$$

with $u \in \{0, 1, \ldots, N_x - 1\}$ and $v \in \{0, 1, \ldots, N_y - 1\}$. We denote the discrete version $\tilde{m}_{\ell,k}(r_x^u, r_y^v)$ as $\tilde{m}_{\ell,k}(u, v)$ for short. This brings us to the discrete form of Theorem 1:

Theorem 2 For an ideal coil configuration, isotropic SPIONs with instantaneous relaxation behavior, even K_x, odd K_y, an equidistant time sampling by Eq. (9), and a spatial sampling by Eq. (10), the following symmetries hold for all components of two-dimensional signal functions

$$\begin{aligned} \tilde{m}_{\ell,k}(N_x - 1 - u, v) &= (-1)^{k+\ell} \tilde{m}_{\ell,k}(u, v), & k \in \mathbb{N}_0, \\ \tilde{m}_{\ell,k}(u, N_y - 1 - v) &= (-1)^{k+\ell} \left(\tilde{m}_{\ell,k}(u, v)\right)^*, & k \in \mathbb{N}_0. \end{aligned} \tag{11}$$

II.III. Transformation with symmetric and antisymmetric basis vectors

We consider the compression of the system matrix $\hat{\boldsymbol{S}}$ by applying a real-valued separable spatial transform $\boldsymbol{T} = \boldsymbol{B}_x \otimes \boldsymbol{B}_y$, where $\otimes$ denotes the Kronecker product. We now prove that the transformed matrix $\hat{\boldsymbol{S}}_{\boldsymbol{T}} = \hat{\boldsymbol{S}}\boldsymbol{T}$ systematically contains zeros when the transforms $\boldsymbol{B}_x$ and $\boldsymbol{B}_y$ applied in x- and y-direction contain only symmetric and antisymmetric basis vectors. In the proof, the transform is separately performed on each system function component $\hat{s}_{\ell,k}(u,v) = \hat{a}_{\ell,k}\tilde{m}_{\ell,k}(u,v)$. We express the signal function component $\tilde{m}_{\ell,k}(u,v)$ as

$$\boldsymbol{M}_{\ell,k} = \begin{pmatrix} \tilde{m}_{\ell,k}(0,0) & \cdots & \tilde{m}_{\ell,k}(N_x-1,0) \\ \vdots & \ddots & \vdots \\ \tilde{m}_{\ell,k}(0,N_y-1) & \cdots & \tilde{m}_{\ell,k}(N_x-1,N_y-1) \end{pmatrix}. \tag{12}$$

We say that the symmetry holds for a basis vector $\boldsymbol{b} = (b_0, b_1, \ldots, b_{L-1})^T$ with $L \in \mathbb{N}$ when the coefficients satisfy

$$b_n = (-1)^\alpha\, b_{L-1-n}. \tag{13}$$

For $\alpha = 0$, $\boldsymbol{b}$ is symmetric, for $\alpha = 1$, it is antisymmetric.

For convenience, we use the notations $\tilde{m}_{\ell,k}(\cdot,v)$ and $\tilde{m}_{\ell,k}(u,\cdot)$ to express vectors with fixed v and u, respectively. Using Eq. (11) and Eq. (13), the scalar product between $\tilde{m}_{\ell,k}(\cdot,v)$ and $\boldsymbol{b}$ with $L = N_x$ for an even N_x is written as

$$\begin{aligned}
&\left\langle \boldsymbol{b}, \tilde{m}_{\ell,k}(\cdot,v)\right\rangle = \sum_{u=0}^{N_x-1} b_u \tilde{m}_{\ell,k}(u,v) \\
&= \sum_{u=0}^{\frac{N_x}{2}-1} b_u \tilde{m}_{\ell,k}(u,v) + \sum_{u=\frac{N_x}{2}}^{N_x-1} b_u \tilde{m}_{\ell,k}(u,v) \\
&= \sum_{u=0}^{\frac{N_x}{2}-1} b_u \tilde{m}_{\ell,k}(u,v) + \sum_{u=0}^{\frac{N_x}{2}-1} b_{N_x-1-u} \tilde{m}_{\ell,k}(N_x-1-u,v) \\
&= \sum_{u=0}^{\frac{N_x}{2}-1} b_u \tilde{m}_{\ell,k}(u,v) + (-1)^{k+\ell} \sum_{u=0}^{\frac{N_x}{2}-1} b_{N_x-1-u} \tilde{m}_{\ell,k}(u,v) \\
&= \sum_{u=0}^{\frac{N_x}{2}-1} \left(b_u + (-1)^{k+\ell}\, b_{N_x-1-u}\right) \tilde{m}_{\ell,k}(u,v) \\
&= \sum_{u=0}^{\frac{N_x}{2}-1} \left[1 + (-1)^{k+\ell+\alpha}\right] b_u \tilde{m}_{\ell,k}(u,v).
\end{aligned} \tag{14}$$

Then, two different cases follow (eight, if we distinguish between k, α and ℓ):

$$\begin{aligned}
\left|\left\langle \boldsymbol{b}, \tilde{m}_{\ell,k}(\cdot,v)\right\rangle\right| &\geq 0 \quad \text{, if } k+\alpha+\ell \text{ is even,} \\
\left|\left\langle \boldsymbol{b}, \tilde{m}_{\ell,k}(\cdot,v)\right\rangle\right| &= 0 \quad \text{, if } k+\alpha+\ell \text{ is odd.}
\end{aligned} \tag{15}$$

Similarly, the scalar product in v-direction between $\boldsymbol{b}$ and $\tilde{m}_{\ell,k}(u,\cdot)$ with $L = N_y$ and an even N_y can be written as

$$\begin{aligned}
&\left\langle \boldsymbol{b}, \tilde{m}_{\ell,k}(u,\cdot)\right\rangle = \sum_{v=0}^{N_y-1} b_v \tilde{m}_{\ell,k}(u,v) \\
&= \sum_{v=0}^{\frac{N_y}{2}-1} b_v \tilde{m}_{\ell,k}(u,v) + \sum_{v=\frac{N_y}{2}}^{N_y-1} b_v \tilde{m}_{\ell,k}(u,v) \\
&= \sum_{v=0}^{\frac{N_y}{2}-1} b_v \tilde{m}_{\ell,k}(u,v) + \sum_{v=0}^{\frac{N_y}{2}-1} b_{N_y-1-v} \tilde{m}_{\ell,k}\left(u,N_y-1-v\right) \\
&= \sum_{v=0}^{\frac{N_y}{2}-1} b_v \left[\tilde{m}_{\ell,k}(u,v) + (-1)^\alpha \tilde{m}_{\ell,k}\left(u,N_y-1-v\right)\right] \\
&= \sum_{v=0}^{\frac{N_y}{2}-1} b_v \left[\tilde{m}_{\ell,k}(u,v) + (-1)^{k+\ell+\alpha} \left(\tilde{m}_{\ell,k}(u,v)\right)^*\right].
\end{aligned} \tag{16}$$

Again, two different cases follow:

$$\begin{aligned}
\Im\left\{\left\langle \boldsymbol{b}, \tilde{m}_{\ell,k}(u,\cdot)\right\rangle\right\} &= 0 \quad \text{, if } k+\alpha+\ell \text{ is even,} \\
\Re\left\{\left\langle \boldsymbol{b}, \tilde{m}_{\ell,k}(u,\cdot)\right\rangle\right\} &= 0 \quad \text{, if } k+\alpha+\ell \text{ is odd.}
\end{aligned} \tag{17}$$

For N_x or N_y being odd, the proofs are derived similarly.

Now we have all necessary properties and can determine what will occur under the transform $\boldsymbol{b}_y^T \boldsymbol{M}_{\ell,k} \boldsymbol{b}_x$. Since the spatial transforms are separable, the symmetries in x- and y-direction do not influence one another. Next, we formulate our results in a lemma.

Lemma If Theorem 2 is fulfilled and $\boldsymbol{b}_x \in \mathbb{R}^{N_x}$ and $\boldsymbol{b}_y \in \mathbb{R}^{N_y}$ both have symmetries defined by $\alpha_x, \alpha_y \in \{0,1\}$ and Eq. (13), then one of the following three different cases will occur:

$$\begin{aligned}
\boldsymbol{b}_y^T \boldsymbol{M}_{\ell,k} \boldsymbol{b}_x &= 0 \text{ if } k+\alpha_x+\ell \text{ odd}\,, \\
\Re\left[\boldsymbol{b}_y^T \boldsymbol{M}_{\ell,k} \boldsymbol{b}_x\right] &= 0 \text{ if } k+\alpha_x+\ell \text{ even} \wedge k+\alpha_y+\ell \text{ odd}, \\
\Im\left[\boldsymbol{b}_y^T \boldsymbol{M}_{\ell,k} \boldsymbol{b}_x\right] &= 0 \text{ if } k+\alpha_x+\ell \wedge k+\alpha_y+\ell \text{ both even.}
\end{aligned} \tag{18}$$

If $\boldsymbol{B}_y \in \mathbb{R}^{N_y \times N_y}$ and $\boldsymbol{B}_x \in \mathbb{R}^{N_x \times N_x}$ have only symmetric and antisymmetric basis vectors and we apply the transfer function $\hat{a}_{\ell,k}$ and vectorize $\hat{a}_{\ell,k} \boldsymbol{B}_y^T \boldsymbol{M}_{\ell,k} \boldsymbol{B}_x$ for each k, at least half of the coefficients in the transformed system matrix $\hat{\boldsymbol{S}}_T \in \mathbb{C}^{N_t \times N_y \cdot N_x}$ are zeros. The purely real and imaginary parts turn into complex ones, because the transfer function $\hat{a}_{\ell,k} = |\hat{a}_{\ell,k}| e^{\mathrm{i}\phi_{\ell,k}}$ is complex valued. In measured system matrices, the phases $\phi_{\ell,k}$ can be approximately estimated under the assumption that the symmetry rules in Theorem 2 are valid for the signal function component (see also [4]). For measured system matrices we cannot expect perfect symmetries and exactly zero values after the transform, because of noise in the measured system matrix.

10.18416/ijmpi.2016.1607002

II.IV. Optimized orthogonal transform

For the compression scheme proposed in this work, the frequency ratio is chosen to be rational with $f_x/f_y = K_y/K_x = K_y/(K_y-1)$, where $K_y \in \mathbb{N}$ is odd in order to fulfill Theorem 2. While the DCT-II and the DTT automatically satisfy the symmetry requirements, they are not yet optimal for compression purposes. We show that better compression can be achieved by applying a secondary orthogonal transform to the matrix $\hat{\boldsymbol{S}}_{\boldsymbol{T}} = \hat{\boldsymbol{S}}\boldsymbol{T}$. This transform must be chosen in such a way that it preserves the symmetries of the basis vectors in $\boldsymbol{B}_x$ and $\boldsymbol{B}_y$. Let $\boldsymbol{B}$ be a placeholder for $\boldsymbol{B}_x$ and $\boldsymbol{B}_y$. We arrange $\boldsymbol{B}$ as $\boldsymbol{B} = [\boldsymbol{b}_0^s, \boldsymbol{b}_1^s, \dots, \boldsymbol{b}_J^s, \boldsymbol{b}_{J+1}^a, \dots, \boldsymbol{b}_{N-2}^a, \boldsymbol{b}_{N-1}^a]$, where $\boldsymbol{b}_l^s$ is symmetric and $\boldsymbol{b}_l^a$ is antisymmetric. Let $\boldsymbol{B}\boldsymbol{R}_{\boldsymbol{q}}(\alpha_{\boldsymbol{q}})$ with $\boldsymbol{q} = (i,j)$ denote a rotation between the i-th and j-th columns of $\boldsymbol{B}$ by an angle $\alpha_{\boldsymbol{q}}$. We choose i and j in such a way that the corresponding columns are either both symmetric $(i,j \in \mathbb{S} = \{0,\dots,J\})$ or antisymmetric $(i,j \in \mathbb{A} = \{J+1,\dots,N-1\})$. These rotations will finally preserve the symmetries. Now let $\boldsymbol{q}_l^x \in \mathbb{A}\times\mathbb{A}$ denote the coordinates for the l-th rotation of antisymmetric basis vectors and $\boldsymbol{p}_i^x \in \mathbb{S}\times\mathbb{S}$ the coordinates for the i-th rotation of symmetric basis vectors, then, for all k, the transform in the x-direction is described by

$$\boldsymbol{T}_x = \boldsymbol{B}_x \prod_{l=1}^{L_a^x} \boldsymbol{R}_{\boldsymbol{q}_l^x}(\alpha_{\boldsymbol{q}_l^x}) \prod_{i=1}^{L_s^x} \boldsymbol{R}_{\boldsymbol{p}_i^x}(\alpha_{\boldsymbol{p}_i^x}) \text{ with } L_a^x, L_s^x \in \mathbb{N}, \quad (19)$$

where L_a^x and L_s^x denote the number of rotations between two antisymmetric and symmetric basis vectors in $\boldsymbol{B}_x$, respectively. To optimize the compression properties, the coordinates $\boldsymbol{q}_l^x$ and $\boldsymbol{p}_i^x$ and the corresponding angles $\alpha_{\boldsymbol{q}_l^x}$ and $\alpha_{\boldsymbol{p}_i^x}$, respectively, are used as free parameters within an optimization framework. The transform $\boldsymbol{T}_y$ in y-direction can be found in a similar fashion. The final transform then reads $\boldsymbol{T} = \boldsymbol{T}_x \otimes \boldsymbol{T}_y$. If the first transforms $\boldsymbol{B}_x$ and $\boldsymbol{B}_y$ are orthogonal, then the final transform $\boldsymbol{T}$ will be orthogonal, because a rotation is an orthogonal transform. In order to promote sparsity, the objective function to be minimized is chosen as $Q = \left\|\mathrm{vec}\left[\hat{\boldsymbol{S}}_{\boldsymbol{T}}\right]\right\|_1$, where the operator vec[·] vectorizes a matrix. The matrix $\boldsymbol{T}$ is parameterized by a set of rotation angles $\left(\alpha_{\boldsymbol{q}_1^x}, \dots, \alpha_{\boldsymbol{q}_{L_a^x}^x}, \alpha_{\boldsymbol{p}_1^x}, \dots, \alpha_{\boldsymbol{p}_{L_s^x}^x}, \alpha_{\boldsymbol{q}_1^y}, \dots, \alpha_{\boldsymbol{q}_{L_a^y}^y}, \alpha_{\boldsymbol{p}_1^y}, \dots, \alpha_{\boldsymbol{p}_{L_s^y}^y}\right)$. However, since optimizing all angles jointly is a highly nonlinear and computationally demanding problem, we consider an alternative approach in which we recursively build up $\boldsymbol{T}$ as

$$\boldsymbol{T}^{i+1} = \boldsymbol{T}^i \cdot \left(\boldsymbol{R}_{\boldsymbol{q}_i^x}(\alpha_{\boldsymbol{q}_i^x})\boldsymbol{R}_{\boldsymbol{p}_i^x}(\alpha_{\boldsymbol{p}_i^x}) \otimes \boldsymbol{R}_{\boldsymbol{q}_i^y}(\alpha_{\boldsymbol{q}_i^y})\boldsymbol{R}_{\boldsymbol{p}_i^y}(\alpha_{\boldsymbol{p}_i^y})\right), \quad (20)$$

with $\boldsymbol{T}^0 = \boldsymbol{B}_x \otimes \boldsymbol{B}_y$. In each step i, the angles for randomly chosen index pairs $\boldsymbol{q}_i^x, \boldsymbol{p}_i^x, \boldsymbol{q}_i^y, \boldsymbol{p}_i^y$ within their sets $\mathbb{A}$ and $\mathbb{S}$ are optimized with a quasi-Newton method to maximally decrease the objective function Q defined above. Finally, it should be mentioned that all rotations can be performed by a full matrix multiplication with the final $\boldsymbol{T}$.

III. Results

For testing, we used a dataset from the Philips MPI mice scanner [5]. This dataset was also used in several related publications [4, 6–8]. In this dataset, the frequencies f_x and f_y were chosen as $f_x = (2.5/96)$ MHz and $f_y = (2.5/99)$ MHz, respectively, resulting in a frequency ratio for the Lissajous trajectory of $f_x/f_y = 33/32$. The sampling rate f_s was 20 MHz. Several frequencies were deleted and only the first 1268 frequency components were available, because it was considered that frequency components higher than 1 MHz only contain noise. The FOV size is 20.4 mm × 12.0 mm and has a 68 × 40 grid.

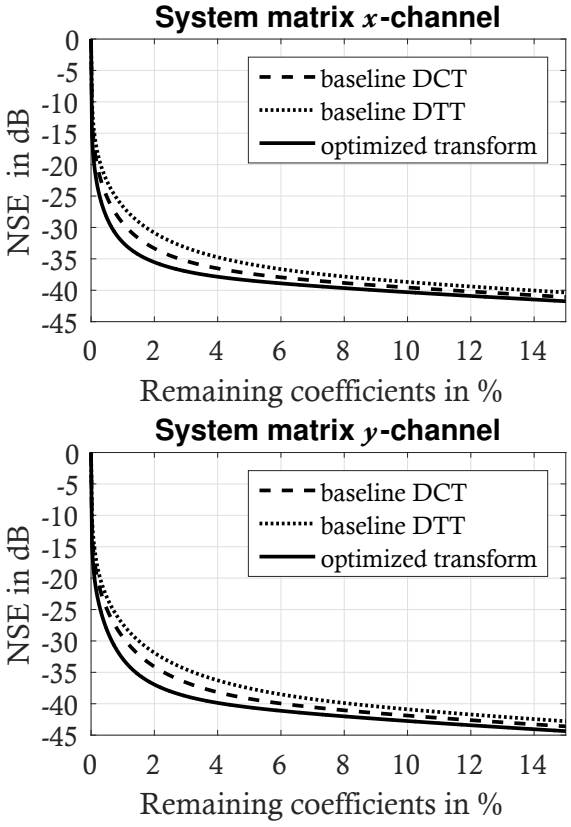

Figure 1: NSE as a function of the percentage of remaining coefficients after global hard-thresholding in the range of 0% to 15%.

For this dataset, we optimized the secondary transform matrices as described above. The first transform matrices $\boldsymbol{B}_x$ and $\boldsymbol{B}_y$ were chosen as DCT-II matrices. As can be seen in Fig. 1, our method obtains better compression ratios in terms of normalized squared error (NSE) than the standard approaches from [3], where the normalized squared error is defined by

$$\epsilon(\boldsymbol{x}, \boldsymbol{x}_c) = \frac{\|\boldsymbol{x}_c - \boldsymbol{x}\|_2^2}{\|\boldsymbol{x}\|_2^2},$$

where $\boldsymbol{x}$ is the original signal and $\boldsymbol{x}_c$ is the reconstructed

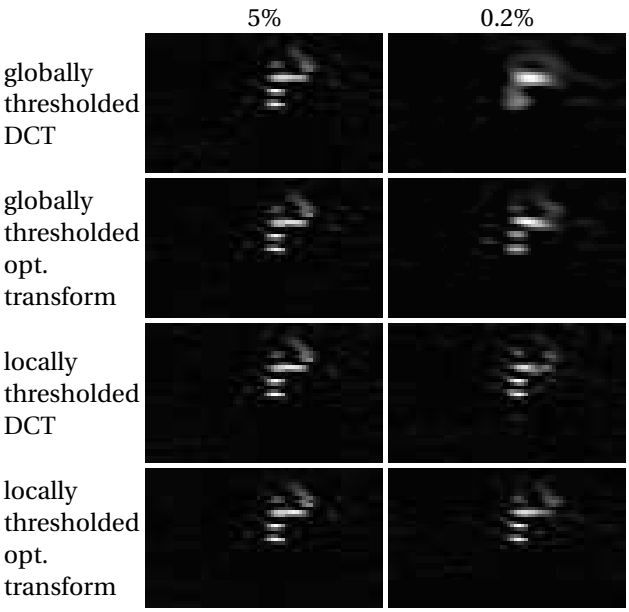

Figure 2: Reconstruction results for global and local thresholds with 0.2% and 5% remaining coefficients and different transforms.

version after lossy compression. One can see that gains of up to 2 dB can be achieved.

In a second experiment we tested the image reconstruction with the compressed system matrix with global [3] and local thresholding [7] strategies. To be comparable to the results in [7] we selected in total 1400 matrix rows from the system matrices related to both receive channels with the best signal-to-noise ratios and concatenated them to one system matrix. Then we thresholded the remaining compressed system matrix so that either 0.2% or 5% of the entries were unequal zero. In Fig. 2 we reconstruct the particle distribution for one frame. As baselines we show also the results for the globally and locally thresholded system matrix compressed by the DCT-II. For our optimized orthogonal transform, we perform global and local thresholding. Like in [7] for 5% remaining coefficients the reconstructed images have similar visual quality. For strong compression with only 0.2% of the original coefficients remaining, the locally thresholded DCT-II results in a heavily blurred version of the P, whereas our optimized transform is still able to reconstruct the particle distribution with just little blur. For the local thresholding with the DCT-II as transform, the reconstruction of the particle distribution results in a smaller blurred version than the global thresholded version of our optimized transform, but with some new artifacts close to the particles. The local threshold reconstruction with our optimized transform is still comparable to the one with 5%, with some additional artifacts close to the particles.

IV. Discussion

We have shown that the applied spatial transforms should obey certain symmetries to ensure sparsity for the transformed system matrix. Experimentally it was verified that these symmetries can be used to compress measured datasets. We show how better compression results for system matrices could be achieved by using an optimized secondary transform that keeps the symmetries of the DCT-II. In a second experiment, we were able to demonstrate that the proposed system matrix compression leads to better reconstruction result than the DCT-II. The reason is that the optimized transform retains more important information on the system matrix than standard transforms. Interestingly, the method cannot be directly transferred to three-dimensional MPI, because no symmetries in all excitation directions can be found (cf. Discussion in [4]), but it is still possible to optimize the transform with help of rotation matrices.

V. Acknowledgments

This work was supported by the German Research Foundation under grant numbers ME 1170/7-1 and BU 1436/7-1.

References

[1] B. Gleich and J. Weizenecker. Tomographic imaging using the nonlinear response of magnetic particles. *Nature*, 435(7046):1214–1217, 2005. doi:10.1038/nature03808.

[2] T. Knopp and T. M. Buzug. *Magnetic Particle Imaging: An Introduction to Imaging Principles and Scanner Instrumentation*. Springer, Berlin/Heidelberg, 2012. doi:10.1007/978-3-642-04199-0.

[3] J. Lampe, C. Bassoy, J. Rahmer, J. Weizenecker, H. Voss, B. Gleich, and J. Borgert. Fast reconstruction in magnetic particle imaging. *Phys. Med. Biol.*, 57(4):1113–1134, 2012. doi:10.1088/0031-9155/57/4/1113.

[4] A. Weber and T. Knopp. Symmetries of the 2d magnetic particle imaging system matrix. *Phys. Med. Biol.*, 60(10):4033, 2015. doi:10.1088/0031-9155/60/10/4033.

[5] J. Weizenecker, B. Gleich, J. Rahmer, H. Dahnke, and J. Borgert. Three-dimensional real-time *in vivo* magnetic particle imaging. *Phys. Med. Biol.*, 54(5):L1–L10, 2009. doi:10.1088/0031-9155/54/5/L01.

[6] T. Knopp and A. Weber. Sparse reconstruction of the magnetic particle imaging system matrix. *IEEE Trans. Med. Imag.*, 32(8):1473–1480, 2013. doi:10.1109/tmi.2013.2258029.

[7] T. Knopp and A. Weber. Local system matrix compression for efficient reconstruction in magnetic particle imaging. *Adv. Math. Phys.*, 2015:472818, 2015. doi:10.1155/2015/472818.

[8] A. Weber and T. Knopp. Reconstruction of the magnetic particle imaging system matrix using symmetries and compressed sensing. *Adv. Math. Phys.*, 2015:460496, 2015. doi:10.1155/2015/460496.